PHYSICAL REVIEW C **87**, 061901(R) (2013)

Azimuthal anisotropy in a jet absorption model with fluctuating initial geometry in heavy ion collisions

Jiangyong Jia

Department of Chemistry, Stony Brook University, Stony Brook, New York 11794, USA
and Physics Department, Brookhaven National Laboratory, Upton, New York 11796, USA

(Received 26 March 2012; revised manuscript received 5 May 2013; published 10 June 2013)

The azimuthal anisotropy due to path-length-dependent jet energy loss is studied in a simple jet absorption model that includes event-by-event fluctuating Glauber geometry. Significant anisotropy coefficients v_n are observed for $n = 1$, 2, and 3, but they are very small for $n > 3$. These coefficients are expected to result in a ridge for correlations between two independently produced jets. The correlations between the orientation of the nth-order anisotropy induced by jet absorption (Φ_n^{QP}) and the nth-order participant plane (Φ_n^{PP}) responsible for harmonic flow are studied. Tight correlations are observed for $n = 2$ in mid-central collisions, but they weaken significantly for $n \neq 2$. The correlations are positive for $n \leqslant 3$, but become negative in central collisions for $n > 3$. The dispersion between Φ_n^{QP} and Φ_n^{PP} is expected to break the factorization of the Fourier coefficients from two-particle correlation $v_{n,n}$ into the single particle v_n, and has important implications for the high-p_{T} ridge phenomena.

DOI: 10.1103/PhysRevC.87.061901 PACS number(s): 25.75.Dw, 25.75.Gz, 24.10.Jv, 24.60.Ky

Introduction. Recently, a great deal of attention is focused on the study of the azimuthal anisotropy of the particle production in heavy ion collisions at the Relativistic Heavy Ion Collider (RHIC) and the Large Hadron Collider (LHC). This anisotropy is usually expanded into a Fourier series

$$\frac{dN}{d\phi} \propto 1 + 2\sum_{n=1}^{\infty} v_n \cos n(\phi - \Phi_n) \tag{1}$$

with v_n and Φ_n representing the magnitude and direction of nth-order anisotropy, respectively. At low p_{T}, v_n is thought to be driven by the anisotropic pressure gradient associated with the initial spatial asymmetries, with more particles emitted in the direction of largest gradients [1]. Asymmetries giving rise to nonzero v_n are associated with either average shape (for $n = 2$) or shapes arising from spatial fluctuations of the participating nucleons [2–5]. They can be characterized by a set of multipole components (also known as eccentricities), calculated from the participating nucleons at (r, ϕ) [3]

$$\epsilon_n = \frac{\sqrt{\langle r^2 \cos n\phi\rangle^2 + \langle r^2 \sin n\phi\rangle^2}}{\langle r^2\rangle}. \tag{2}$$

The orientations of the minor axis for each moment n, also known as the participant plane (PP) are given by

$$\Phi_n^{\mathrm{PP}} = \frac{\mathrm{atan2}(\langle r^2 \sin n\phi\rangle, \langle r^2 \cos n\phi\rangle)}{n} + \frac{\pi}{n}. \tag{3}$$

When fluctuations are small and linearized hydrodynamics is applicable, each v_n is expected to be independently driven by ϵ_n along $\Phi_n^{\mathrm{PP}} = \Phi_n$ [3]. This may not be true when the fluctuations are large, as the nonlinear effects may lead to significant mixing between harmonic flows of different order [6]. In this paper, linear hydrodynamics are assumed ($\Phi_n^{\mathrm{PP}} = \Phi_n$) in order to facilitate the study of the correlations between Φ_n of different physics origins.

At high p_{T} ($p_{\mathrm{T}} \gtrsim 10$) GeV, the v_n is thought to be driven by the path-length-dependent energy loss of jets traversing the medium, with more particles emitted along the direction of shortest path length, Φ_n^{QP} (QP stands for "quenching plane", the direction of minimal jet attenuation) [7,8]. Since jet quenching is influenced by the same geometry as for flow, the direction of smallest jet attenuation is expected to be correlated with the direction of largest pressure gradient for flow. In fact, these two directions are often implicitly assumed to be the same in many theoretical calculations [9–14]. An explicit study of the correlation between these directions can help clarify this assumption.

In this paper, we estimate the high-p_{T} anisotropy coefficients v_n and Φ_n^{QP} using a jet absorption model with event-by-event fluctuating Glauber geometry. In multijet events with multiple hard-scattering processes, we show that the attenuation of jet yield leads to collimation of jet pairs at small relative angles and results in a near-side ridge in two-particle correlations (2PC) at high p_{T}. We study the correlations between Φ_n^{PP} and Φ_n^{QP}, and show explicitly that these two angles are not the same. We explain how this angle misalignment influences the relation between the high-p_{T} ridge and high-p_{T} v_n. The experimental prospect for measuring the high-p_{T} ridge is discussed in our model framework.

Model. We use a simple jet-absorption–Glauber model of Ref. [15] to calculate v_n and Φ_n^{QP}. This model has been used previously to study the centrality and path-length dependence of single particle suppression R_{AA}, dihadron suppression I_{AA}, and v_2. Back-to-back jet pairs are generated according to the binary collision density profile (ρ_c) in the transverse (xy) plane with random orientation. They are then propagated through the medium, whose density is given by the participant density profile (ρ_p). Both profiles are generated with a Monte Carlo Glauber model with event-by-event fluctuation of positions of nucleons in Au ions [16]. The nucleons are sampled from a Woods-Saxon distribution with a radius of 6.38 fm and diffuseness of 0.535 fm, with a nucleon-nucleon cross section of $\sigma_{\mathrm{nn}} = 42$ mb. In order to have smooth distributions for ρ_c and ρ_p, the nucleons are assumed to have a Gaussian profile

 ©2013 American Physical Society

in transverse plane with a width of $r_0 = 0.4$ fm in x and y direction similar to Ref. [10]. The value of r_0 is varied from 0.2–0.4 fm, and the nucleon is also assumed to be a uniform disk with a radius of $\sqrt{\sigma_{\rm nn}/\pi}/2 = 0.58$ fm. However the final results are found to be insensitive to the details of the nucleon shape, except in peripheral collisions.

The jet quenching is implemented via exponential attenuation $f = e^{-\kappa I}$ for midrapidity, where the matter integral I is calculated as

$$I_m = \int_0^\infty dl \frac{l^m}{l+l_0} \rho(\overrightarrow{\mathbf{r}} + (l+l_0)\widehat{\mathbf{v}}) \tag{4}$$

$$\approx \int_0^\infty dl\ l^{m-1}\ \rho(\overrightarrow{\mathbf{r}} + l\widehat{\mathbf{v}}), \quad m = 1, 2 \tag{5}$$

for jet generated at $\overrightarrow{\mathbf{r}} = (x, y)$ and propagated along direction $\widehat{\mathbf{v}}$ with the same speed. They correspond to l^{m+1} dependence of absorption ($\propto l^m dl$) in a longitudinal expanding or 1+1D medium ($\propto 1/(l_0 + l)$ or 1D Hubble expansion) with a thermalization time of $l_0 = c\tau_0$. The l_0 is fixed to 0 by default, but we have checked that the v_n does not change much for $l_0 < 0.3$ fm [10]. The two cases, $m = 1$ and $m = 2$, are motivated for the l dependence expected for radiative and AdS/CFT energy loss in 1+1D medium [17,18], respectively.

The absorption coefficient κ controls the jet quenching strength and is the only parameter in this calculation. It is tuned to reproduce $R_{\rm AA} = \langle e^{-\kappa I_m}\rangle \sim 0.19$ for 0-5% π^0 data at RHIC after averaging over many Glauber events [19]. This leads to a value of $\kappa = 0.1473$ fm^{-1} and 0.0968 fm^{-2} for $m = 1$ and 2, respectively.

Results. Figure 1 summarizes the basic information obtained from this procedure for one typical Au-Au event in 0–5% centrality interval. Figures 1(a) and 1(b) show the density profile for ρ_p and ρ_c, respectively. Figure 1(c) shows the normalized probability distribution of I_1: $P[I_1(\phi)]$, which is obtained by calculating I_1 over all possible di-jet production points ρ_c and jet propagation direction ϕ. This distribution exhibits characteristic high-density and low-density regions in (I_1, ϕ) space, presumably reflecting spatial correlation between the ρ_c and ρ_p profiles. Figure 1(d) shows the normalized probability distribution of the attenuation $e^{-\kappa I_1}$. Figure 1(e) shows the $\langle e^{-\kappa I_1}\rangle$ averaged along the y axis in Fig. 1(d) as a function ϕ, which is precisely the azimuthal angle-dependent suppression $R_{\rm AA}(\phi)$. A clear anticorrelation can be seen between the peak magnitude of the $R_{\rm AA}(\phi)$ and breadth of the I_1 distribution in Fig. 1(c). This distribution can also be obtained by randomly generating many di-jet pairs according the ρ_c and propagating them through ρ_p via Eq. (6). We expand it into a Fourier series

$$R_{\rm AA}(\phi) = R^0_{\rm AA}\left[1 + 2\sum_{n=1}^{\infty} v_n^{\rm QP} \cos n\left(\phi - \Phi_n^{\rm QP}\right)\right], \tag{6}$$

where $R^0_{\rm AA}$ represents the average suppression, $v_n^{\rm QP}$ and $\Phi_n^{\rm QP}$ represent the magnitude and direction of nth-order harmonic of emission probability distribution, respectively. Similar studies

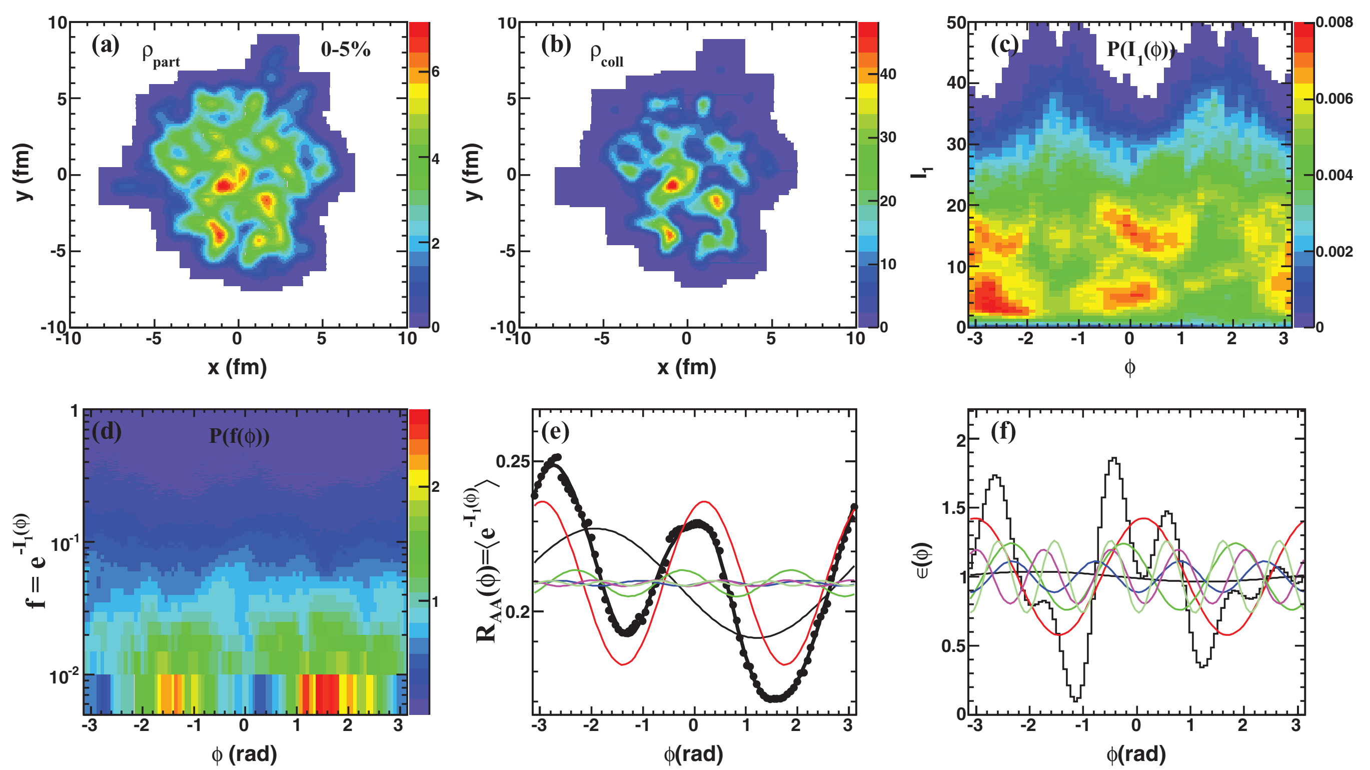

FIG. 1. (Color online) The complete set of output obtained in the jet absorption model for one event in 0–5% centrality interval: (a) the participant density profile (ρ_p); (b) the collision density profile (ρ_c); (c) the probability distribution of the path-length integral I_1; (d) the probability distribution of jet surviving the exponential attenuation; (e) the distribution of survival rate as function of azimuth angle; (f) the initial spatial asymmetry of the participants calculated via Eq. (7). The original impact parameter of the event is aligned along the x axis.

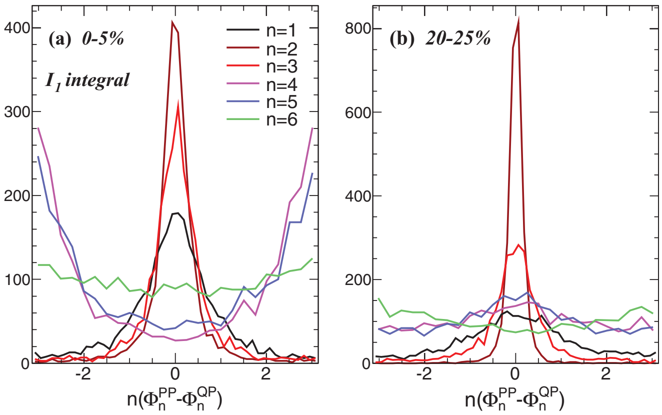

FIG. 2. (Color online) The correlation between participant plane Φ_n^{PP} and quenching plane Φ_n^{QP} with $n = 1$–6 calculated for I_1 path-length dependence and for (a) 0–5% and (b) 20–25% centrality interval.

of $R_{\mathrm{AA}}(\phi)$ were pursued before in Ref. [12] for a pQCD energy loss in an event-by-event hydrodynamic underlying event. However it focused primarily on the influence of fluctuations on the event-averaged $R_{\mathrm{AA}}(\phi)$ distribution relative to the second-order event plane (EP).

Figure 1(f) shows a distribution calculated from ϵ_n and Φ_n^{QP},

$$\epsilon(\phi) = 1 + 2\sum_{n=1}^{\infty} \epsilon_n \cos n\big(\phi - \Phi_n^{\mathrm{PP}}\big). \tag{7}$$

It visualizes the shape of the initial geometry that is transformed into the final momentum anisotropy via either flow or jet quenching. A good alignment is seen between Φ_n^{PP} and Φ_n^{QP} for $n \leqslant 3$. It also shows that the large ϵ_n for $n > 3$ are strongly damped after jet absorption, leading to very small values of v_n^{QP} for $n > 3$.

The study shown in Fig. 1 can be repeated for many events. We divide the simulation data into 5% centrality intervals, each containing about 2500 events. Figure 2 shows the distribution of Φ_n^{PP}–Φ_n^{QP} for two centrality intervals. Strong positive correlations are obtained for $n = 1$, 2, and 3, while the correlations are rather weak or even become negative for $n > 3$.[1]

In heavy ion collisions at RHIC and LHC, the v_n is usually measured from particle distribution relative to Φ_n via Eq. (1) [20]. However it has also been derived from the Fourier coefficients of two-particle correlation in relative azimuthal angle $\Delta\phi = \phi^{\mathrm{a}} - \phi^{\mathrm{b}}$ [21]

$$\frac{dN_{\mathrm{pairs}}}{d\Delta\phi} \propto 1 + 2\sum_{n=1}^{\infty} v_{n,n}\big(p_{\mathrm{T}}^{\mathrm{a}}, p_{\mathrm{T}}^{\mathrm{b}}\big)\cos n\Delta\phi, \tag{8}$$

with

$$v_{n,n}\big(p_{\mathrm{T}}^{\mathrm{a}}, p_{\mathrm{T}}^{\mathrm{b}}\big) = v_n\big(p_{\mathrm{T}}^{\mathrm{a}}\big)v_n\big(p_{\mathrm{T}}^{\mathrm{b}}\big). \tag{9}$$

[1] Φ_n^{PP} in Eq. (3) is calculated with r^2 weighting. We have also repeated the study using r^n weighting for $n > 1$ and r^3 weighting for $n = 1$ [5], but very little differences are seen.

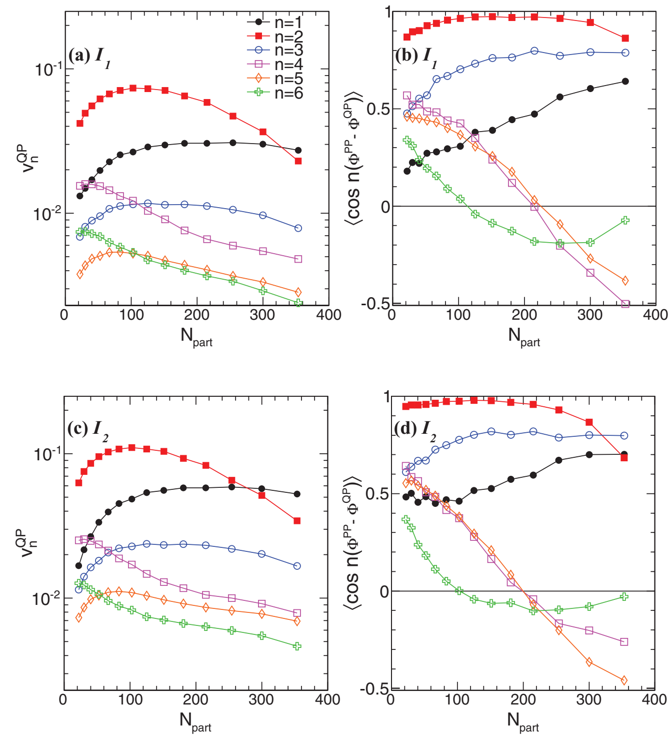

FIG. 3. (Color online) The centrality dependence of anisotropy coefficients v_n^{QP} (left panels) and correlation between the participant plane and quenching plane $\langle\cos n(\Phi_n^{\mathrm{PP}} - \Phi_n^{\mathrm{QP}})\rangle$ (right panels) for I_1 type of path-length dependence (top panels) and I_2 types of path-length dependence (bottom panels). Note that the values of v_n^{QP} are positive by construction according to Eq. (6).

The fact that the quenching plane and participant plane do not align exactly with each other implies that the v_n measured relative to Φ_n^{PP} is not the same as those contributing to the 2PC in Eq. (8). In other words, it is possible that the v_n obtained from single particle analysis is only a fraction of the true anisotropy resulting from jet quenching

$$v_n = v_n^{\mathrm{QP}}\big\langle\cos n\big(\Phi_n^{\mathrm{PP}} - \Phi_n^{\mathrm{QP}}\big)\big\rangle. \tag{10}$$

Since what is measured in experiment is the event plane not the PP, it is important to check whether the event plane aligns with QP or not, for example in a hydrodynamic model calculation.

Figures 3(a) and 3(c) summarize the centrality dependence of v_n^{QP} with $n = 1$–6 and for I_1 and I_2, respectively. Significant v_n^{QP} signals are observed for $n \leqslant 3$, while higher-order v_n^{QP} are usually smaller than 1%. The v_2^{QP} and v_4^{QP}–v_6^{QP} all show strong centrality dependence, while the v_1^{QP} and v_3^{QP} show little centrality dependence for $N_{\mathrm{part}} > 100$. Interestingly, the value of the v_1^{QP} is consistently larger than that for v_3^{QP}, and it even exceeds v_2^{QP} value in most central collisions. This behavior suggests that the path-length dependence of energy loss and initial dipole asymmetry from fluctuations combine to produce a large v_1^{QP}. This large v_1^{QP} is expected to contribute to the high-p_{T} v_1 signal observed by the ATLAS Collaboration [21]. Figure 3 also shows that the I_2 type of path-length dependence induces significantly larger v_n^{QP} than that for I_1: the increase

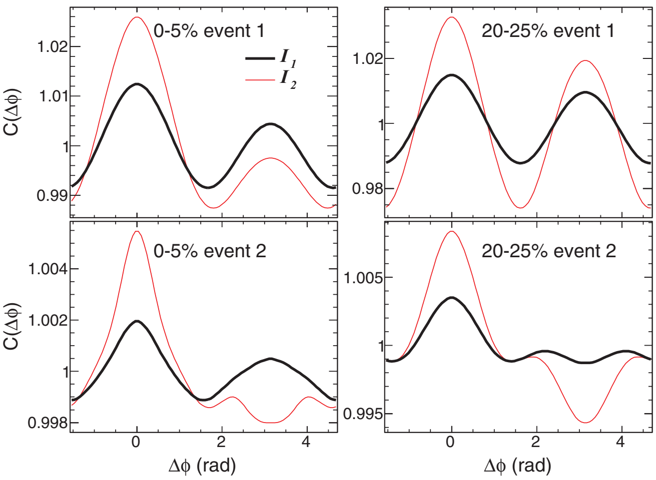

FIG. 4. (Color online) The expected long-range structures for correlations between two high-p_T particles from independent hard-scattering processes. They are shown for two typical events in 0–5% centrality interval (left panels) and 20–25% centrality interval (right panels); each of them should be regarded as the distributions obtained for many events with identical initial geometry.

is almost a factor of two for $n = 1$ and $n = 3$. This is also observed in other studies before [10,18].

Figures 3(b) and 3(d) summarize the centrality dependence of $\langle \cos n(\Phi_n^{\rm PP} - \Phi_n^{\rm QP})\rangle$ with $n = 1$–6 and for I_1 and I_2, respectively. As indicated by Eq. (10), this represents the reduction factor of the v_n when it is measured relative to the $\Phi_n^{\rm PP}$. The reduction is small for $n = 2$, except in central collisions where it reaches 15% for I_1 and 30% for I_2. However the reduction is significantly larger for $n = 1$ and 3, reaching about 50% for $n = 1$ in mid-central collisions. The $\langle \cos n(\Phi_n^{\rm PP} - \Phi_n^{\rm QP})\rangle$ value becomes negative for $n > 3$ in central collisions, reflecting an anticorrelation between $\Phi_n^{\rm PP}$ and $\Phi_n^{\rm QP}$ (already shown in Fig. 2). Interestingly, $\langle \cos n(\Phi_n^{\rm PP} - \Phi_n^{\rm QP})\rangle$ values for $n = 1$ are always smaller than that for $n = 3$ (more misalignment), while $v_1^{\rm QP}$ is always larger than $v_3^{\rm QP}$.

The dispersion between the $\Phi_n^{\rm QP}$ and $\Phi_n^{\rm PP}$ has important implications on the factorization relation Eq. (9). The factorization of $v_{n,n}$ into v_n is obviously valid for correlations between two low p_T particles (soft-soft correlation) as both are modulated around $\Phi_n^{\rm PP}$. The factorization should also be valid for correlation between a low-p_T particle and a high-p_T particle (soft-hard correlation) since it involves the projection of the v_n onto $\Phi_n^{\rm PP}$, i.e., $v_{n,n}(p_T^a, p_T^b) = v_n(p_T^a) v_n^{\rm QP}(p_T^b)\langle \cos n(\Phi_n^{\rm PP} - \Phi_n^{\rm QP})\rangle = v_n(p_T^a) v_n(p_T^b)$. Experimental data indeed support this [21,23]. However the correlation between two high-p_T particles from two independent hard-scattering processes (hard-hard correlation) is expected to be larger than the product of the two single particle v_n

$$v_{n,n}(p_T^a, p_T^b) = v_n^{\rm QP}(p_T^a) v_n^{\rm QP}(p_T^b) = \frac{v_n(p_T^a) v_n(p_T^b)}{\left\langle \cos n\left(\Phi_n^{\rm PP} - \Phi_n^{\rm QP}\right)\right\rangle^2}. \tag{11}$$

Therefore, the factorization can not work simultaneously for soft-soft, soft-hard, and hard-hard correlations.

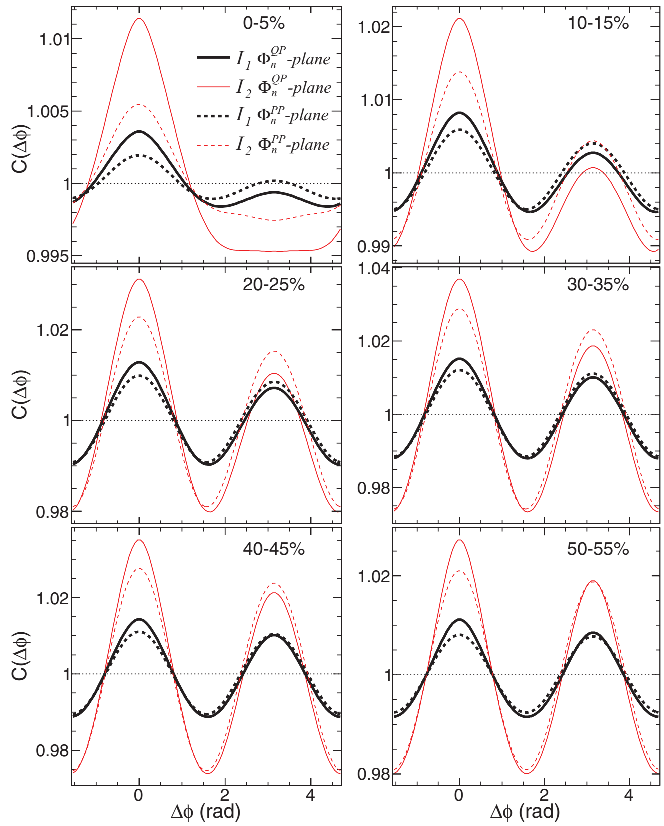

FIG. 5. (Color online) The expected long-range structures for correlations between two high p_T particles from two independent hard-scattering processes (solid lines) and those calculated from single particle $v_n^{\rm QP}$ relative to participant planes (dashed lines) for various centrality intervals. They are average distribution over many events for a given centrality intervals. The thick (thin) lines denote the I_1 (I_2) type of path-length dependence.

The large anisotropy coefficients $v_n^{\rm QP}$ also has important consequences for the ridge observed in two-particle correlations [21–23]. This ridge is thought to be the result of the constructive contribution of harmonics at $\Delta\phi \sim 0$. In the literature, it is referred to as either the soft ridge [24,25] for soft-soft correlation or hard ridge [22,26] for soft-hard correlation, respectively. Here we show that the correlation between two independently produced high-p_T jets can also produce the ridgelike structure. This hard-hard ridge can be calculated on a probability basis event-by-event by simply self-convoluting the $R_{AA}(\phi)$ distribution as in Fig. 1(e). Examples of these structures are shown in Fig. 4 for two representative events in both 0–5% and 20–25% centrality intervals. The magnitude of the ridge, as well as the away-side shape changes dramatically from event to event. They also change a lot between the I_1 and I_2 types of path-length dependence jet absorption.

Figure 5 show the long-range structures (solid lines) obtained from the jet absorption model, averaged over many events. The ridge magnitude increases with centrality to about 1.5% (4%) for I_1 (I_2) path-length dependence in mid-central collisions. This signal should be measurable with the large statistics data set from LHC. The dashed lines in Fig. 5 show the 2PC predicted from the v_n measured relative to Φ_n^{PP}. Clearly the misalignments between Φ_n^{QP} and Φ_n^{PP} reduces the ridge magnitude. The reduction is almost 50% in most central collisions, but decrease to about 20% in mid-central collisions. This suggests the difference between the measured ridge and those predicted by the event plane method could be large and measurable.

Conclusion. The anisotropy of high-p_{T} particle is studied in a simple jet absorption framework with event-by-event fluctuating geometry. The harmonic coefficients v_n are found to be significant for $n = 1$–3 ($>1\%$) but become very small for $n > 3$. The correlation between the quenching plane and participant plane are studied. A strong decorrelation is found for $n = 2$ in central collisions and for $n = 1$ and 3 over the full centrality range. The correlations become negative for $n > 3$ in central collisions. This decorrelation, if also confirmed between the event plane and the quenching plane (e.g., via hydrodynamic model that has dijets embedded), is expected to break the global factorization of the two-particle Fourier coefficient $v_{n,n}$ into the v_n for the two single particles. It would also imply that the high-p_{T} v_n measured relative to the event plane could be significantly smaller than the true anisotropy from path-length-dependent jet energy loss. These jet quenching v_n also give rise to long-range ridge structures in two-particle correlations. The predicted ridge amplitude is on the order of 0.5–4% depending on the centrality and functional form of the l dependence of the energy loss, and should be measurable at the LHC using the correlations between two high-p_{T} particles with a large rapidity separation. Our study bears some similarities to Ref. [14]. However, Ref. [14] uses a cumulant expansion framework instead of Monte Carlo Glauber model for initial geometry, and it focuses on the soft-hard ridge instead of the hard-hard ridge in our case.

Acknowledgments. Discussions with Jinfeng Liao are acknowledged. This research is supported by NSF under Grant No. PHY-1019387.

[1] J. Y. Ollitrault, Phys. Rev. D **46**, 229 (1992).
[2] B. Alver and G. Roland, Phys. Rev. C **81**, 054905 (2010); **82**, 039903(E) (2010).
[3] B. H. Alver, C. Gombeaud, M. Luzum, and J.-Y. Ollitrault, Phys. Rev. C **82**, 034913 (2010).
[4] P. Staig and E. Shuryak, Phys. Rev. C **84**, 034908 (2011).
[5] D. Teaney and L. Yan, Phys. Rev. C **83**, 064904 (2011).
[6] Z. Qiu and U. W. Heinz, Phys. Rev. C **84**, 024911 (2011).
[7] M. Gyulassy, I. Vitev, and X. N. Wang, Phys. Rev. Lett. **86**, 2537 (2001).
[8] PHENIX Collaboration, Phys. Rev. Lett. **105**, 142301 (2010).
[9] S. A. Bass, C. Gale, A. Majumder, C. Nonaka, G.-Y. Qin, T. Renk, and J. Ruppert, Phys. Rev. C **79**, 024901 (2009).
[10] J. Jia and R. Wei, Phys. Rev. C **82**, 024902 (2010).
[11] J. Jia, W. A. Horowitz, and J. Liao, Phys. Rev. C **84**, 034904 (2011).
[12] T. Renk, H. Holopainen, J. Auvinen, and K. J. Eskola, Phys. Rev. C **85**, 044915 (2012).
[13] B. Betz, M. Gyulassy, and G. Torrieri, Phys. Rev. C **84**, 024913 (2011).
[14] X. Zhang and J. Liao, Phys. Lett. B **713**, 35 (2012); J. Liao and E. Shuryak, Phys. Rev. Lett. **102**, 202302 (2009).
[15] A. Drees, H. Feng, and J. Jia, Phys. Rev. C **71**, 034909 (2005).
[16] B. Alver, M. Baker, C. Loizides, and P. Steinberg, arXiv:0805.4411 [nucl-ex].
[17] P. M. Chesler, K. Jensen, A. Karch, and L. G. Yaffe, Phys. Rev. D **79**, 125015 (2009).
[18] C. Marquet and T. Renk, Phys. Lett. B **685**, 270 (2010).
[19] A. Adare *et al.*, Phys. Rev. Lett. **101**, 232301 (2008).
[20] A. M. Poskanzer and S. A. Voloshin, Phys. Rev. C **58**, 1671 (1998).
[21] ATLAS Collaboration, Phys. Rev. C **86**, 014907 (2012).
[22] STAR Collaboration, Phys. Rev. C **80**, 064912 (2009).
[23] CMS Collaboration, Eur. Phys. J. C **72**, 2012 (2012).
[24] STAR Collaboration, J. Phys. G **35**, 104090 (2008).
[25] S. Gavin, L. McLerran, and G. Moschelli, Phys. Rev. C **79**, 051902 (2009).
[26] G. Moschelli and S. Gavin, Nucl. Phys. A **830**, 623C (2009).